Estimation of Forest Leaf Area Index Using Vegetation Indices Derived From Hyperion Hyperspectral Data

Peng Gong, Ruiliang Pu, Greg S. Biging, and Mirta Rosa Larrieu

***Abstract*—Field spectrometer data and leaf area index (LAI) measurements were collected on the same day as the Earth Observing 1 satellite overpass for a study site in the Patagonia region of Argentina. We first simulated the total at-sensor radiances using MODTRAN 4 for atmospheric correction. Then ground spectroradiometric measurements were used to improve the retrieved reflectance for each pixel on the Hyperion image. Using the improved pixel-based surface reflectance spectra, 12 two-band "vegetation indices (VIs)" were constructed using all available 168 Hyperion bands. Finally, we evaluated the correlation of each possible vegetation index with LAI measurements to determine the most effective bands for forest LAI estimation. The experimental results indicate that most of the important hyperspectral bands with high R^2 are related to bands in the shortwave infrared (SWIR) region and some in the near-infrared (NIR) region. The bands are centered near 820, 1040, 1200, 1250, 1650, 2100, and 2260 nm with bandwidths ranging from 10–300 nm. It is notable that the originally defined VIs that use red and NIR bands did not produce higher correlation with LAI than VIs constructed with bands in SWIR and NIR regions.**

***Index Terms*—Hyperion, hyperspectral data, leaf area index (LAI), shortwave infrared (SWIR), vegetation index.**

I. Introduction

LEAF AREA index (LAI) is defined as the total one-sided area of all leaves in the canopy within a defined region (m^2/m^2). LAI is an important structural parameter for quantifying the energy and mass exchange characteristics of terrestrial ecosystems such as photosynthesis, respiration, transpiration, carbon and nutrient cycle, and rainfall interception (e.g., [1]–[6]). Direct measure of canopy LAI is relatively accurate but extremely labor intensive and destructive. Thus, it is practical to measure LAI only on limited experimental plots. Consequently, field estimation of LAI over large areas is problematic. Remote sensing techniques, particularly the use of satellite imagery, have been used to measure LAI on a landscape scale or even global scale [7]. With remote sensing techniques, scientists have made progress in developing methods that correlate remotely sensed data with regional estimates of a number of forest ecosystem variables, including LAI, absorbed fraction of photosynthetically active radiation (APAR), canopy temperature, and community type. In the past three decades, the traditional broadband vegetation indices (VIs), such as the Thematic Mapper (TM)-derived normalized difference vegetation index (NDVI), have been widely applied to estimate canopy LAI (e.g., [1], [2], [8], and [9]). The broadband indices, usually constructed with near-infrared (NIR) and red (R) bands, use average spectral information over broad bandwidths, resulting in loss of critical information available in specific narrow bands [10]. In addition, the broadband indices are known to be heavily affected by soil background at low vegetation cover [11], [12].

The advent of imaging spectrometers on board aircraft has made it possible to construct more refined VIs through the use of distinct narrow bands. Narrow bands can be crucial for providing additional information over broad bands in quantifying biophysical characteristics of vegetation [13]. For instance, TM band 3 (630–690 nm, R band) and TM band 4 (760–900 nm, NIR band) can be further separated into six and 14 Airborne Visible/Infrared Imaging Spectrometer (AVIRIS) narrow bands, respectively. It is possible to improve the indices by using some of the distinct narrow bands for correction of soil background effects. Earth Observing 1 (EO-1) is the world's first satellite that carries a hyperspectral sensor—Hyperion [35], which has the same spatial resolution as TM. In this study, we evaluate 12 VIs, constructed with bands across the Hyperion spectral range of 0.4–2.5 μm to find some important bands with potential for improving LAI estimation at the landscape level.

II. Background

In studies of forest ecosystems with remote sensing data, the most commonly used vegetation indices are computed from simple functions based on the R and NIR bands. Reflectances in R and NIR wavebands, denoted ρ_{NIR} and ρ_{R} have been used to formulate various vegetation indices (VIs) as indicators of surface vegetation conditions (e.g., [1], [11], and [14]). Among the various VIs (Table I), the ratio-based NDVI [15], and the simple ratio vegetation index (SR) [16] are the most frequently used to correlate with LAI and other canopy structure parameters from airborne and spaceborne remoter sensing data (e.g., [2], [9], and [17]). With increases in LAI, red reflectance decreases as light is absorbed by leaf pigments (such as chlorophylls), while the NIR signal increases as more leaf layers are present to scatter the radiation upward [2] because plant

Manuscript received May 24, 2002; revised January 7, 2003. This research was supported in part by the National Aeronautics and Space Administration under Earth Observing 1 Science Validation Grant NCC5-492, and field support was provided by the Forest Plantation Inventory Section of the Secretariat of Agriculture, Livestock, Fisheries and Food of the government of Argentina.

P. Gong, R. Pu, and G. S. Biging are with the Center for Assessment and Monitoring of Forest and Environmental Resources (CAMFER), University of California, Berkeley, CA 94720-3110 USA (e-mail: rpu@nature.berkeley.edu).

M. R. Larrieu is with the Proyecto Forestal de Desarrollo, Secretaría de Agricultura, Ganaderìa, Pesca y Alimentación, 1063 Buenos Aires, Argentina.

Digital Object Identifier 10.1109/TGRS.2003.812910

TABLE I
SUMMARY OF 12 TWO-BAND VEGETATION INDICES ANALYZED IN THIS STUDY. NOTE: ρ_{R} AND ρ_{NIR} ARE DENOTED AS REFLECTANCES IN R AND NIR WAVELENGTHS, BUT IN THIS STUDY THEY REPRESENT BANDS 1 AND 2 ACROSS ALL AVAILABLE 168 BANDS OF HYPERION DATA

Index	Formula	Description	References (e.g.)
SR	ρ_{NIR} / ρ_R	Near-infrared / Red rreflectance ratio (Simple Ratio VI). Related to changes in amount of green biomass, pigment content and concentraion and leaf water stress etc.	Baret and Guyot, 1991; Tucher, 1979.
NDVI	$(\rho_{NIR} - \rho_R)/(\rho_{NIR} + \rho_R)$	Normalized Difference Vegetation Index. Related to changes in amount of green biomass, pigment content and concentraion and leaf water stress etc.	Fassnacht et al., 1997; Smith et al., 1991.
PVI	$\frac{1}{\sqrt{a^2+1}}(\rho_{NIR} - a\rho_R - b)$ a = slope of the soil line b = soil line intercept	Perpendicular Vegetation Index, orthogonal to the soil line. Attempts to eliminate differences in soil background and is most effective under conditions of low LAI, applicable for arid and semiarid regions.	Baret and Guyot, 1991; Huete et al., 1985.
SAVI	$\frac{(\rho_{NIR} - \rho_R)(1+L)}{(\rho_{NIR} + \rho_R + L)}$ L = a correction factor	Soil Adjusted Vegetation Index. L ranges from 0 for very high vegetation cover to 1 for very low vegetation cover; minimizes soil brightness-induced variations L=0.5 can reduce soil noise problems for a wide range of LAI.	Huete, 1988; Leeuwen and Huete, 1996.
NLI	$(\rho_{NIR}^2 - \rho_R)/(\rho_{NIR}^2 + \rho_R)$	Non-Linear vegetation Index. Consider the relationship between many VIs and surface biophysical parameters is often nonlinear, and NLI linearizes relationships with surface parameters that tend to be nonlinear.	Goel and Qin, 1994
RDVI	$(\rho_{NIR} - \rho_R)/(\rho_{NIR} + \rho_R)^{1/2}$	Re-nomalized Difference Vegetation Index. RDVI linearizes relationships with surface parameters that tend to be nonlinear.	Roujean and Breon, 1995.
MSR	$\frac{(\rho_{NIR}/\rho_R - 1)}{(\rho_{NIR}/\rho_R)^{1/2} + 1}$	Modified Simple Ratio. It can be an improvement over RDVI for linearizing the relationships between the index and biophysical parameters.	Chen, 1996.
WDVI	$\rho_{NIR} - a\rho_R$ a = slope of the soil line	Weighted Difference Vegetation Index. WDVI assumes that the ratio between NIR and R reflectances of bare soil is constant; it is related to PVI, but it has an unrestricted range.	Clevers, 1988; Clevers, 1991.
MNLI	$\frac{(\rho_{NIR}^2 - \rho_R)(1+L)}{(\rho_{NIR}^2 + \rho_R + L)}$ L = a correction factor	Modified Non-linear vegetation Index. MNLI is an improved version of NLI, and it also consider merit of SAVI. L=0.5 may be applicable for a wide range of LAI. For detailed description, see text.	Developed in this paper.
NDVI*SR	$\frac{(\rho_{NIR}^2 - \rho_R)}{(\rho_{NIR} + \rho_R^2)}$	Attemps to combine merit of NDVI with that of SR. For detailed description, see text.	Developed in this paper.
SAVI*SR	$\frac{(\rho_{NIR}^2 - \rho_R)}{(\rho_{NIR} + \rho_R + L)\rho_R}$	Attemps to combine merit of SAVI with that of SR. For detailed description, see text.	Developed in this paper.
TSAVI	$\frac{a(\rho_{NIR} - a\rho_R - b)}{[a\rho_{NIR} + \rho_R - ab + X(1+a^2)]}$ a = slope of the soil line b = soil line intercept X = adjustment factor to minimize soil noise.	Transformed Soil Adjusted Vegetation Index. Modify Huete (1988) SAVI to compensate for soil variability due to changes in solar elevation and canopy structure.	Baret and Guyot, 1991;

cell walls—notably the lignin component—cause scattering of NIR energy, resulting in relatively high NIR transmittance and reflectance [18]. However, the VIs are sensitive to optical properties of the soil background. Their application is limited if one does not account for the effects of soil background.

Richardson and Wiegand [19] proposed the perpendicular vegetation index (PVI) in an attempt to reduce the effect of soil background on VIs. However, experimental and theoretical investigations indicate that it is still affected by soil background (e.g., [14] and [20]): brighter soils result in higher index values for a given quantity of incomplete vegetation cover. Additional indices have been proposed to overcome this problem. For instance, an index named weighted difference vegetation index (WDVI) was proposed in [21] and [22]. However, Baret and Guyot [11] found that WDVI held no advantage over PVI. This has led to the development of alternative formulations that include correction factors or constants attempting to account for or minimize the effect of varying background reflectance on VIs. For examples, the soil-adjusted vegetation index (SAVI) developed in [14] was derived from the NDVI, but an adjustment factor L was introduced in order to minimize soil-brightness influences and to produce vegetation isolines more independent of the soil background [11]. Graphically, the SAVI involves a shifting of the origin of reflectance spectra plotted in NIR-R wavelength space to account for the first-order soil—vegetation interactions and differential R and NIR flux extinction through vegetated canopies [14]. The constant L can range from zero (for very high vegetation cover, the corresponding SAVI being equivalent to NDVI) to 1 (for very low vegetation cover). If L tends toward infinity, it is equivalent to PVI. Huete [14] suggested that an adjusted factor $L = 0.5$ for intermediate vegetation amounts should be used, resulting in a spectral index (SAVI) superior to the NDVI and PVI for a relatively wide range of vegetation conditions. In order to further reduce error for a vegetation index (e.g., SAVI) for plant canopies with varying low densities, Baret *et al.* [23] proposed the transformed soil adjusted vegetation index (TSAVI). TSAVI equals zero for bare soil and is close to 0.7 for very dense

canopies. It can compensate for soil variability due to changes in solar elevation and canopy structure.

To simulate nonlinear relationships between VIs and surface biophysical parameters, Goel and Qin [24]–[26] proposed the nonlinear vegetation index (NLI), the renormalized difference vegetation index (RDVI), and the modified simple ratio vegetation index (MSR), respectively. The nonlinear vegetation indices attempt to linearize relationships with surface parameters that tend to be nonlinear. To preserve the merits of existing VIs while improving their performance in LAI estimation, in this study, we also tested three modified or combined VIs from the existing ones. MNLI modifies NLI and incorporates merits of SAVI. Under conditions of low LAI, where ρ_{R} is relatively high and ρ_{NIR} relatively low, a small change in ρ_{R} produces a larger proportional change in NDVI than SR. With higher LAI, in general, where ρ_{NIR} is higher and ρ_{R} lower, a change in ρ_{NIR} will induce a larger proportional change in SR than NDVI [9]. Therefore, the NDVI*SR is expected to balance the two phenomena to increase correlation with LAI, while the SAVI*SR simply combines the merit of SAVI (eliminating effect of soil background) with that of SR (a wider range of VI values corresponding to a narrower range of vegetation cover). All 12 VIs mentioned above were tested in this study and are summarized in Table I.

The 12 VIs were originally constructed only as functions of R and NIR. However, some researchers (e.g., [27]–[30]) also used bands within the SWIR spectral region ($\sim$ 1.0–2.5 μm), especially the ratio of middle-infrared (MIR) (1.55–1.75 μm) to NIR as a new vegetation index. It was hypothesized that the index is correlated to the LAI through the summation of the individual leaf equivalent water thickness for each leaf layer to obtain a total canopy equivalent water thickness [27] because leaf reflectances of the SWIR region are dominated by liquid water absorption. Motivated by this, we will test all 12 VIs across all Hyperion band pairs in spite of violating the original definitions of bands used to compute the VIs, especially for those defined also with a soil line in R-NIR space. In addition, because of their simple definition, explicit underlying physical processes, and extensive use of these two-band VIs, we will focus on the evaluation of these 12 two-band VIs in this study instead of considering VIs constructed with more than two bands. After removing those Hyperion bands with strong water absorption (1346–1447 and 1800–1961 nm) and weak and noisy signal bands (wavelength shorter than 437 nm and longer than 2405 nm), we have 168 Hyperion bands available in this test. We expect that some new two-band VIs, constructed from the 168 bands, may be found that produce higher correlations with forest LAI than currently used VIs.

III. Study Site and Datasets

A. Study Site

During the 2001 EO-1 campaign in Argentina, we established a site (41°10′59″ S/71°20′27″ W) in the Rio Negro province in the Patagonia region of southern Argentina. The study area is a relatively flat semiarid region with conifer forest plantations of young- to mid-aged ponderosa pine, lodgepole pine, and Oregon pine. Other broad-leaf species, shrub, and grasses (mainly consisting of nire brush acaena, coiron, barberis, laura, and rosa mosquede) are also found over this site. The average elevation is 850 m, with variations within 100 m.

B. Data Acquisition and Measurement

Hyperion data were acquired on March 27, 2001, around 10:30 A.M. local time. From March 27–29, 2001, we took reflectance measurements in the field from targets such as road surface (gravel material), bare soil, young tree canopies (ponderosa pine and lodgepole pine), and grasses and shrub using a FieldSpec®Pro FR (Analytical Spectral Devices, Inc.). These spectral reflectance measurements were then used for atmospheric correction for the Hyperion data as described below.

A LAI-2000 Plant Canopy Analyzer (PCA) was used in the field to measure forest LAI. The LAI measurement taken by the PCA is the "effective" LAI [1], [5]. The instructions for operating the LAI instrument were carefully followed to ensure each LAI point was measured accurately. From March 27–29, 2001, a total of 32 LAI measurements were taken. Each LAI measurement represents an average of ten PCA readings that were taken mainly from overstory in an area between 100–1000 m^2. The locations of PCA readings in each plot were selected, based on the canopy closure, age of stands, and nutrient level so as to make them representative of the variability in the plot. Because the LAI measurement plots are all forest plantations, for plots with an LAI > 2.0, almost no understory was found. For plots whose LAI is lower than 2.0, there existed a varying proportion of understory that may contribute to LAI measurement. The understory mostly consists of some broad-leaf species. In consideration of the fact that a Hyperion pixel spectrum always responds to both the understory and overstory, especially for those sparse forests, we did not attempt to separate contributions of the understory and overstory to the LAI measurement in this study. After taking the LAI measurement, its exact location (i.e., a plot) was marked on the color composite image of high spatial resolution AVIRIS data or on a forest inventory polygon map. These were used as references for subsequent spectral data extraction from the Hyperion image. Since the effective LAI is less variable and easier to measure than LAI, is an intrinsic attribute of plant canopies [1], and has also a proportion relation with LAI [36], we directly used the effective LAI throughout this research and referred it to as LAI.

IV. Methods

A. Atmospheric Correction

In this study, we used a hybrid method of atmospheric correction to retrieve surface reflectance from Hyperion data. The sensor measures radiance L that is a combination of the radiance from the surface and scattered from the atmosphere. In a simplified form, the at-sensor radiance, L, can be related to the Lambertian surface reflectance ρ as

$$L = L_a + \frac{T_2 \rho}{1 - \rho S} \cdot \frac{E_s \cdot \cos(\theta_s)}{\pi} \tag{1}$$

where T_2 is the sun-surface sensor two-way transmittance; L_a is the path radiance caused by atmospheric scattering; S is the spherical albedo of the atmosphere; θ_s is the solar zenith angle;

and E_s is the exoatmospheric solar irradiance. Further, rearrange (1) for retrieval of surface reflectance, ρ, as

$$\rho = \frac{L - L_a}{(L - L_a)\,S + T_2 \cdot \frac{E_s \cdot \cos(\theta_s)}{\pi}}. \tag{2}$$

According to (1) and (2), once a satellite-measured radiance L is given and solving (1) for parameters, T_2, S, and L_a through simulation with an atmospherically radioactive transfer code such as MODTRAN 4, a surface reflectance spectrum can be retrieved.

The hybrid method for retrieving surface reflectance from Hyperion data is briefly described as follows. With MODTRAN 4 [31], the simulated output radiance is used as L in (1). With three at-sensor total radiances, we can construct a group of three equations from (1), and solve them for T_2, S, and L_a. Using sensor pixel radiance values as at-sensor radiance and solving T_2, S, and L_a, with (2), we can easily calculate a pixel-based retrieved surface reflectance from the Hyperion image, called as the initial reflectance. With the ground reflectance spectrum and initial reflectance of the same location (target), a set of ratios across all spectral bands is calculated by dividing the ground reflectance by its corresponding initial reflectance. In order to make the ratios more representative of various targets, it is appropriate to use an average ratio calculated from different targets (e.g., road surface and vegetation in this study). Multiplying the initial reflectance of each pixel by its corresponding ratio in each band, we can improve the initial reflectance. We call the ground reflectance corrected reflectance, the improved reflectance.

B. Correlation Analysis of Vegetation Indices Extracted From Hyperion Data With LAI

Pixel-based retrieved reflectance spectra from the calibrated Hyperion images at the 32 LAI measurement plots were extracted from the image. One to four homogenous pixels were extracted and averaged for each LAI plot. The 12 VIs were applied to any possible pair of the 168 Hyperion bands. Note that R bands and NIR bands used for constructing one VIs in Table I have been extended to all 168 bands. Consequently, for each pair of bands we have 12 VIs for each of the 32 LAI measurements.

For each of the 12 VIs, a linear correlation coefficient (R^2) was calculated between the VI and LAI measurement (32 samples). Due to the fact that most LAI measurements are less than five in this study (over which spectral saturation may happen and this in turn will reduce the linear correlation between VI and LAI), a linear R^2 is a suitable indicator for finding some important bands contributing to better correlation between a two-band index and LAI. However, if LAI measurements are higher than five, a nonlinear correlation indicator (e.g., mean square error) maybe more appropriate. In this study, a linear R^2 was adopted as an indicator of effectiveness in correlation analysis. Since each VI in Table I could be constructed from any pair among the possible 168 bands, a linear correlation coefficient (R^2) matrix (e.g., Fig. 1) could be constructed. From the correlation matrices, hyperspectral bands with high correlation coefficients were examined.

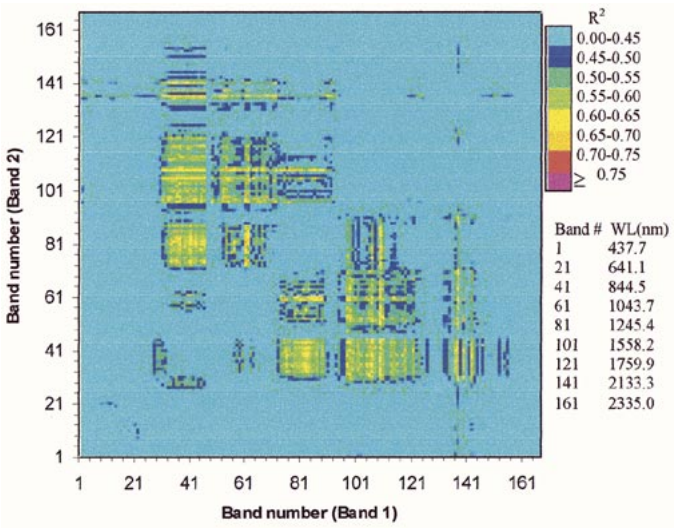

Fig. 1. Color plots showing correlations (R^2) between LAI and NDVI calculated from any band pairs among 168 Hyperion bands spread across 430–2410 nm. Different color areas represent different R^2 class values, which were ranked and from which best band centers and best bandwidths were calculated for the VI used for estimating the forest LAI (Table II).

V. Results and Analysis

A. Atmospheric Correction

Inputs to the MODTRAN 4 included three surface reflectance values, 0.0, 0.3, and 0.5, a water vapor value of 0.7 cm/cm^2, the Midlatitude Summer (45° South Latitude) atmospheric geographical–seasonal model, and other necessary parameters [31]. The total radiances of Hyperion were simulated as an output for solving the simplified radioactive transfer model (1). A water vapor of 0.7 was determined according to the "smoothness test" by [32]. With the three simulated at-sensor total radiances and three surface reflectance values, the path radiance (L_a), the sun-surface sensor two-way transmittance (T_2), and the spherical albedo of atmosphere (S) were obtained by solving the three-equation group of (1). A corrected radiance image (i.e., $L_{\text{img}} - L_a$) was produced by replacing the simulated at-sensor radiance with the image pixel value (suppose $L_{\text{img}} \approx L$) and then subtracting the path radiance L_a. With two other parameters (T_2 and S), the initial surface reflectance image was produced according to (2).

The initial reflectance still has a lot of "spikes" along the reflectance curve. These might be caused by supplying less than optimal input values to MODTRAN 4, especially for those sensitive gases such as water vapor, and also by inadequate simulation of atmospheric conditions during the satellite overpass. It is, therefore, necessary to further modify the initial reflectance with ground spectroradiometeric measurements. We used ground spectrometer data measured from road surface (gravel, four spectra) and plant canopies (lodgepole pine, five spectra) to calibrate the Hyperion image to obtain the conversion ratios, then applied the ratios to the initial reflectance image to produce the improved reflectance image. After the calibration with the ground-based measurements, the improved reflectance curve looks better although some small "spikes" near 0.94 and 1.14 μm still exist due to the residue of the water vapor effect.

TABLE II
POTENTIAL HYPERSPECTRAL BANDS FOR 12 VEGETATION INDICES APPLIED FOR FOREST LAI ESTIMATION. NOTE: Optim. = OPTIMAL CORRELATION R^2. BOLDFACE CHEMICALS ARE PRINCIPAL FOR THE ABSORPTION FEATURES

Index	R^2 NIR-R/Optim.	Band center (nm)	Bandwidth (nm)	Band description (spectral region and possible absorption features)
SR	0.55/0.70	825	140	NIR region, **cell structure** multi-reflected spectra.
		1038	230	NIR-SWIR region, **water**, **proten**, lignin, starch & oil absorption
		1250	180	SWIR region, **water**, cellulose, starch and lignin absorption
		1648	290	SWIR region, **protein**, **nitrogen**, **lignin**, **cellulose**, sugar, starch absorption.
NDVI	0.55/0.70	...	...	4 bands similar to SR's
PVI	0.45/0.64	814	140	NIR region, **cell structure** multi-reflected spectra.
		1050	100	NIR-SWIR region, **proten**, lignin, and oil absorption
		1250	190	SWIR region, **water**, cellulose, starch and lignin absorption
		2100	10	SWIR region, **starch,** cellulose absorption
SAVI	0.50/0.67	...	...	4 bands similar to NDVI's or SR's
NLI	0.50/0.73	821	157	NIR region, **cell structure** multi-reflected spectra.
		1200	578	NIR-SWIR region, **water**, proten, starch, lignin, cellulose, and oil absorption
		1250	191	SWIR region, **water**, cellulose, starch and lignin absorption
		1640	300	SWIR region, **protein**, **nitrogen**, **lignin**, **cellulose**, sugar, starch absorption.
RDVI	0.45/0.66	810	170	NIR region, **cell structure** multi-reflected spectra.
		1054	10	SWIR region, lignin and oil absorption
		1255	161	SWIR region, **water**, cellulose, starch and lignin absorption
		1669	10	SWIR region, lignin and starch absorption
		2093	10	SWIR region, starch and cellulose absorption
MSR	0.50/0.70	...	...	4 bands similar to NDVI's or SR's
WDVI	0.45/0.63	1639	10	SWIR region,non apparent absorption
		2113	10	SWIR region, **starch** and cellulose absorption
		2285	30	SWIR region, starch, cellulose and protein absorption
MNLI	0.45/0.75	...	...	4 bands similar to NLIs
NDVI*SR	0.50/0.71	...	...	4 bands similar to NDVI's or SR's, but
SAVI*SR	0.50/0.71	...	...	1 - 4 bands similar to SAVI's or SR's
		2083	30	SWIR region, sugar, starch and cellulose absorption
		2153	10	SWIR region, protein absorption
TSAVI	0.50/0.71	832	120	NIR region, **cell structure** multi-reflected spectra.
		1038	150	NIR-SWIR region, **water**, **proten**, lignin, starch & oil absorption
		1240	170	SWIR region, **water**, lignin, cellulose and starch absorption
		1660	260	SWIR region, **lignin**, **cellulose, sugar**, starch, protein, and nitrogen absorption.
		2108	20	SWIR region, **starch**, cellulose and protein absorption

B. Correlation of Vegetation Indices With LAI

For each VI, a correlation matrix was constructed for each pair of spectral bands. In the correlation matrix, the color legend indicates the class value of R^2 between the two-band index and LAI. For the 12 correlation matrices, R^2 values for some matrices are symmetrical for the diagonal of the matrix (e.g., NDVI, PVI and SAVI), and others are not (see MNLI, NDVI*SR, SAVI*SR, and TSAVI). From all 12 correlation matrices, some bands (expressed as band centers and bandwidths) having high potential in LAI estimation are summarized in Table II. The R^2 column in the table lists two R^2 values: a highest R^2 value for the actual use of NIR and R bands, selected from all possible VIs between any two NIR and R bands, and an optimal R^2 value derived from VIs constructed from the SWIR and NIR regions.

R^2 matrices for SR, NDVI, and MSR have similar patterns (e.g., Fig. 1 for NVDI). The patches with high R^2 mainly cluster in four band regions centered at 825, 1038, 1250, and 1648 nm with 140–290-nm bandwidths. Compared to the R^2 value calculated from the original VI definition using R and NIR bands, some important band pairs can be found in the NIR and SWIR or the SWIR regions. In particular, some bands in the NIR and MIR regions yielded higher R^2 values. These bands are related to plant leaf water content that has a close correlation with canopy biomass and LAI (Hunt, 1991) and indirectly to the absorption features of protein, nitrogen, lignin, cellulose and starch concentrations. With PVI and WDVI (see Fig. 2 for PVI), we did not find higher R^2 values than those of NDVI and SR. This might be because soil background was simple, i.e., dry, bright and similar among the 32 LAI measurement plots. For WDVI, the upper

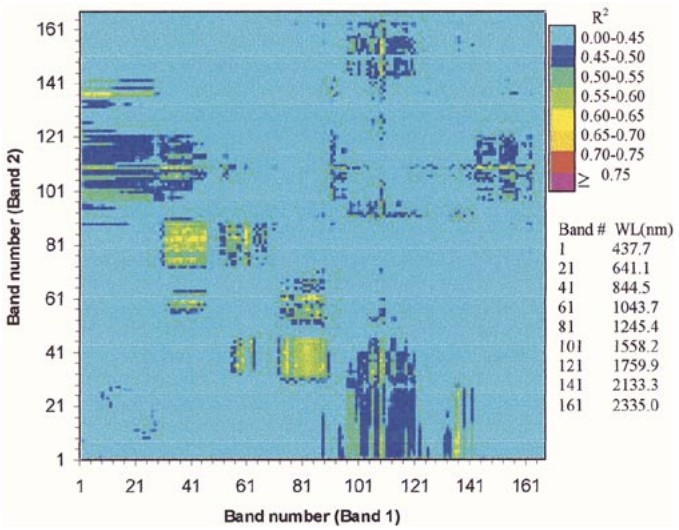

Fig. 2. Color scale plots showing correlations (R^2) between LAI and PVI. More explanation is found in Fig. 1.

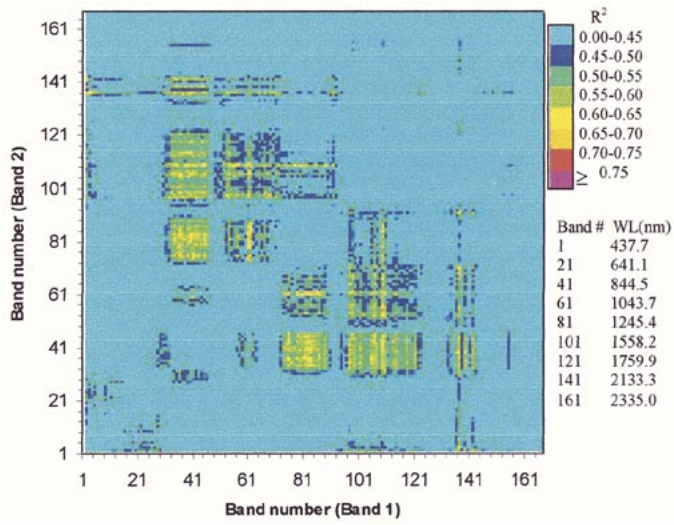

Fig. 3. Color scale plots showing correlations (R^2) between LAI and SAVI. More explanation is found in Fig. 1.

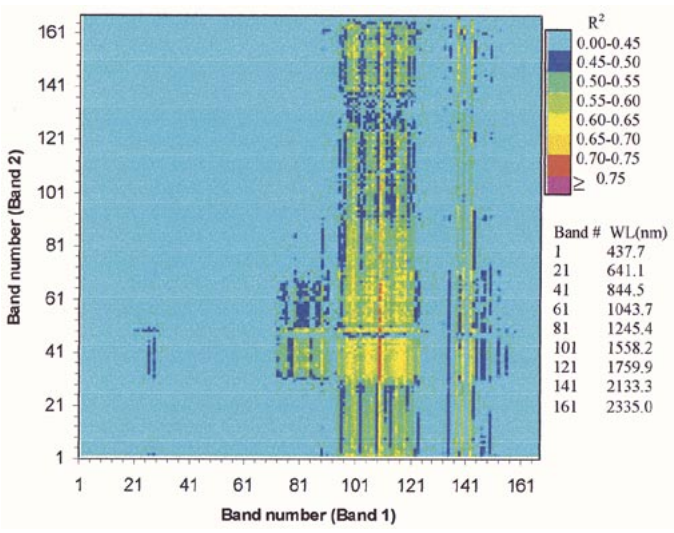

Fig. 4. Color scale plots showing correlations (R^2) between LAI and MNLI. More explanation is found in Fig. 1.

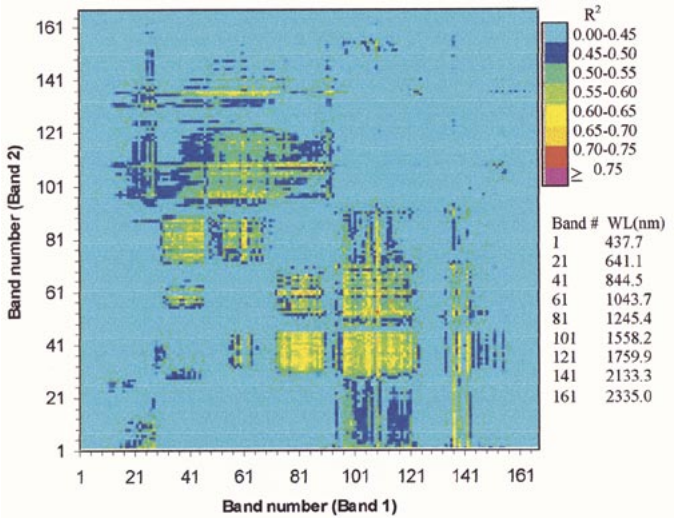

Fig. 5. Color scale plots showing correlations (R^2) between LAI and TSAVI. More explanation is found in Fig. 1.

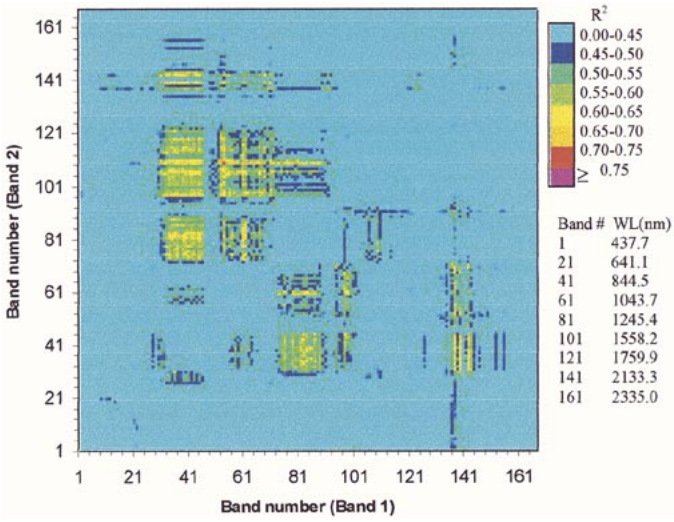

Fig. 6. Color scale plots showing correlations (R^2) between LAI and NDVI*SR. More explanation is found in Fig. 1.

right quarter of the R^2 matrix is similar to that of PVI, which may account for their close relationship [11]. For both PVI and WDVI, some important bands are also found in the SWIR and the NIR and SWIR regions. The R^2 values for SAVI (Fig. 3) are again similar to those of NDVI or SR due to the simple soil background.

NLI and MNLI can linearize the nonlinear relationships with surface parameters. This resulted in an improvement in R^2 values (0.73, 0.75) when compared to that of NDVI (0.70). Their R^2 matrices are not symmetrical along the diagonal. MNLI (Fig. 4), developed in this study, improved the performance (from R^2 0.73 to 0.75) of its original version NLI, especially for wavelengths longer than 1500 nm. The potential bands for estimating forest LAI might be wavelengths centered near 821, 1200, 1250, and 1640 nm with bandwidths from 157–578 nm, which are affected directly or indirectly by water, protein, nitrogen, lignin, cellulose sugar absorption features [33], and cell structure reflection feature. Although RDVI also linearizes the relationships between VI and surface biophysical parameters, it has relatively low correlations. Since the RDVI is a renormalization of NDVI, its R^2 values in the correlation matrix were expected to have similar patterns to those of NDVI. However, we found the correlation levels in the RDVI matrix to be lower than those in the NDVI matrix. For TSAVI, the R^2 values have a similar distribution pattern as those in the SAVI correlation matrix, but the level of correlation is higher than observed with the SAVI (Fig. 5). This may result from the compensation of soil variability due to changes in solar elevation and canopy structure [11]. Some important bands based on the TSAVI correlation matrix include wavelengths centered at 832, 1038, 1240, 1660, and 2108 nm with bandwidths from 20–260 nm.

The remaining two combined indices—NDVI*SR and SAVI*SR (Figs. 6 and 7)—developed in this study have performed slightly better than the original VIs. The R^2 values have different patterns below the diagonals than those in their original VIs. The R^2 values in their correlation matrices,

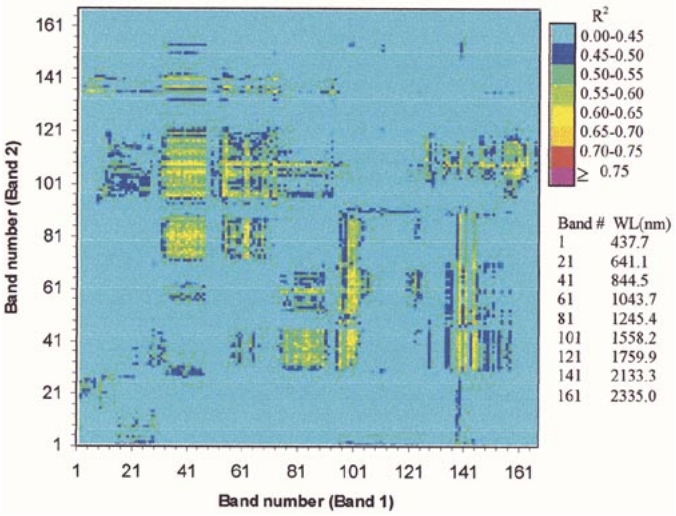

Fig. 7. Color scale plots showing correlations (R^2) between LAI and SAVI*SR. More explanation is found in Fig. 1.

therefore, are not symmetrical. The potential bands for LAI estimation are similar to those found from either the NDVI or the SR matrices.

Based on the experimental results for the 12 VIs constructed from all band pairs across the available 168 Hyperion bands, it is evident that most of the hyperspectral bands producing high correlation with the forest LAI are found in the SWIR region and some in the NIR region. They are centered near 820, 1040, 1200, 1250, 1650, 2100, and 2260 nm with bandwidths ranging from 10–300 nm. The bands used for constructing the VIs for forest LAI estimation are indirectly controlled mainly by plant leaf water content. The absorption features by other biochemicals, such as protein, nitrogen, lignin, cellulose, sugar, and starch, may also indirectly affect the correlation between VIs and LAI [33]. However, the VIs constructed with the R and NIR bands did not produce correlations with LAI as high as those VIs constructed from bands in the SWIR region. This might partly be attributed to the strong interference of the atmosphere with the satellite-based hyperspectral data in the visible wavelengths (mainly Rayleigh and aerosol scattering within visible and NIR regions or wavelength < 1.0 μm) for clear sky conditions [34]. Based on their high correlation with LAI measurements, we suggest that MNLI (NLI), SR, and NDVI be some better VIs that can be used for estimating forest LAI in semiarid environments. This is because MNLI (NLI) can linearize relationships with surface parameters that tend to be nonlinear. SR and NDVI can catch strong spectral differential signals (e.g., spectral difference between high reflection and absorption features caused by cell structure, leaf water content, and other biochemicals).

VI. Conclusion

In this study, we conducted correlation analyses of forest LAI with 12 vegetation indices extracted from Hyperion image reflectances. We constructed 12 different vegetation indices from all possible band pairs in the Hyperion image and then correlated each of them with field LAI measurements. Results indicate that many hyperspectral bands in the SWIR region and some in NIR region have the greatest potential in forming indices for LAI estimation. The most effective band wavelengths centered near 820, 1040, 1200, 1250, 1650, 2100, and 2260 nm with bandwidths ranging from 10–300 nm. These bands are controlled by plant leaf water content, yet the absorption features by other biochemicals such as protein, nitrogen, lignin, cellulose, sugar, and starch may have indirect impacts. VIs derived from the R and NIR bands did not produce as high correlations with LAI as those with bands in the SWIR and NIR regions. Based on their high correlation with LAI measurements, MNLI (NLI), SR, and NDVI were recommended for use in environments similar to our study site for LAI estimation using satellite-based hyperspectral data.

Acknowledgment

Assistance in field work by G. Defossé, F. Farías, and M. C. Frugoni is greatly appreciated.

References

[1] J. Chen and J. Cihlar, "Retrieving leaf area index of boreal conifer forests using Landsat TM images," *Remote Sens. Environ.*, vol. 55, pp. 153–162, 1996.

[2] K. S. Fassnacht, S. T. Gower, M. D. MacKenzie, E. V. Nordheim, and T. M. Lillesand, "Estimating the leaf area index of north central Wisconsin forests using the Landsat Thematic Mapper," *Remote Sens. Environ.*, vol. 61, pp. 229–245, 1997.

[3] N. Gobron, B. Pinty, and M. M. Verstraete, "Theoretical limits to the estimation of the leaf area index on the basis of visible and near-infrared remote sensing data," *IEEE Trans. Geosci. Remote Sensing*, vol. 35, pp. 1438–1445, Nov. 1997.

[4] P. Gong, R. Pu, and J. R. Miller, "Coniferous forest leaf area index estimation along the Oregon transect using compact airborne spectrographic imager data," *Photogramm. Eng. Remote Sens.*, vol. 61, no. 9, pp. 1107–1117, 1995.

[5] J. D. White, S. W. Running, R. Nemani, R. E. Keane, and K. C. Ryan, "Measurement and remote sensing of LAI in Rocky Mountain montane ecosystems," *Can. J. Forest Res.*, vol. 27, pp. 1714–1727, 1997.

[6] B. Hu, K. Inannen, and J. R. Miller, "Retrieval of leaf area index and canopy closure from CASI data over the BOREAS flux tower sites," *Remote Sens. Environ.*, vol. 74, pp. 255–274, 2000.

[7] S. W. Running, R. R. Nemani, D. L. Peterson, L. E. Band, D. F. Potts, L. L. Pierce, and M. A. Spanner, "Mapping regional forest evapotranspiration and photosynthesis by coupling satellite data with ecosystem simulation," *Ecology*, vol. 70, no. 4, pp. 1090–1101, 1989.

[8] C. J. Tucker, "Red and photographic infrared linear combinations for monitoring vegetation," *Remote Sens. Environ.*, vol. 8, pp. 127–150, 1979.

[9] D. P. Turner, W. B. Cohen, R. E. Kennedy, K. S. Fassnacht, and J. M. Briggs, "Relationships between leaf area index and Landsat TM spectral vegetation indices across three temperate zone sites," *Remote Sens. Environ.*, vol. 70, pp. 52–68, 1999.

[10] G. A. Blackburn, "Quantifying chlorophylls and caroteniods at leaf and canopy scales: An evaluation of some hyperspectral approaches," *Remote Sens. Environ.*, vol. 66, pp. 273–285, 1998.

[11] F. Baret and G. Guyot, "Potentials and limits of vegetation indices for LAI and APAR assessment," *Remote Sens. Environ.*, vol. 35, pp. 161–173, 1991.

[12] C. D. Elvidge and R. J. P. Lyon, "Influence of rock-soil spectral variation on the assessment of green biomass," *Remote Sens. Environ.*, vol. 17, pp. 265–269, 1985.

[13] P. S. Thenkabail, R. B. Smith, and E. D. Pauw, "Hyperspectral vegetation indices and their relationships with agricultural crop characteristics," *Remote Sens. Environ.*, vol. 71, pp. 158–182, 2000.

[14] A. R. Huete, "A soil adjusted vegetation index (SAVI)," *Remote Sens. Environ.*, vol. 25, pp. 295–309, 1988.

[15] J. W. Rouse, R. H. Haas, J. A. Schell, and D. W. Deering, "Monitoring vegetation systems in the Great plains with ERTS," in *Proc. 3rd ERTS Symp.*, vol. 1, 1973, pp. 48–62.

[16] C. F. Jordan, "Derivation of leaf area index from quality of light on the forest floor," *Ecology*, vol. 50, pp. 663–666, 1969.

[17] P. W. Treitz and P. J. Howarth, "Hyperspectral remote sensing for estimating biophysical parameters of forest ecosystems," *Progr. Phys. Geography*, vol. 23, no. 3, pp. 359–390, 1999.

[18] D. Gate, J. J. Keegan, J. C. Schleter, and V. R. Weidner, "Spectral properties of plant," *Appl. Opt.*, vol. 4, pp. 11–20, 1965.
[19] A. J. Richardson and C. L. Wiegand, "Distinguishing vegetation from soil background information," *Photogramm. Eng. Remote Sens.*, vol. 43, pp. 1541–1552, 1977.
[20] D. J. Major, F. Baret, and G. Guyot, "A ratio vegetation index adjusted for soil brightness," *Int. J. Remote Sensing*, vol. 11, no. 5, pp. 727–740, 1990.
[21] J. G. P. W. Clevers, "Application of the WDVI in estimating LAI at the generative stage of barley," *ISPRS J. Photogramm. Remote Sens.*, vol. 46, pp. 37–47, 1991.
[22] ——, "The derivation of a simplified reflectance model for the estimation of leaf area index," *Remote Sens. Environ.*, vol. 25, pp. 53–69, 1988.
[23] F. Baret, G. Guyot, and D. Major, "TSAVI: A vegetation index which minimizes soil brightness effects on LAI and APAR estimation," in *Proc. 12th Can. Symp. Remote Sensing and IGARSS'90*, Vancouver, BC, Canada, July 10–14, 1989, pp. 1–4.
[24] N. S. Goel and W. Qi, "Influences of canopy architecture on relationships between various vegetation indices and LAI and FPAR: A computer simulation," *Remote Sens. Rev.*, vol. 10, pp. 309–347, 1994.
[25] J. -L. Roujean and E. M. Breon, "Estmating PAR absorbed by vegetation from bibirectional reflectance measurements," *Remote Sens. Environ.*, vol. 51, pp. 375–384, 1995.
[26] J. M. Chen, "Evaluation of vegetation indices and a modified simple ratio for boreal applications," *Can. J. Remote Sens.*, vol. 22, pp. 229–242, 1996.
[27] E. R. Hunt Jr., "Airborne remote sensing of canopy water thickness scaled from leaf spectrometer data," *Int. J. Remote Sens.*, vol. 12, no. 3, pp. 643–649, 1991.
[28] R. R. Nemani, L. L. Pierce, S. W. Running, and L. E. Band, "Forest ecosystem processes at the watershed scale: Sensitivity to remotely-sensed leaf area index estimates," *Int. J. Remote Sens.*, vol. 14, no. 13, pp. 2519–2534, 1993.
[29] P. J. Curran and H. D. Williamson, "GLAI estimation using measurements of red, near infrared and middle infrared radiance," *Photogramm. Eng. Remote Sens.*, vol. 53, pp. 181–186, 1987.
[30] D. L. Peterson, M. A. Spanner, S. W. Running, and K. B. Tueber, "Relationship of thematic mapper simulator data to leaf area index of temperature coniferous forests," *Remote Sens. Environ.*, vol. 22, pp. 323–341, 1987.
[31] A. Berk, G. P. Anderson, P. K. Acharya, J. H. Chetwynd, L. S. Bernstein, E. P. Shettle, M. W. Matthew, and S. M. Adler-Golden, *MODTRAN4 User's Manual*. Hanscom AFB, MA: Air Force Res. Lab., 2000, pp. 1–93.
[32] Z. Qu, A. F. H. Goetz, and K. B. Heidebrecht, "High-accuracy Atmosphere Correction for Hyperspectral data (HATCH)," in *Proc. AVIRIS 2000 Workshop*, 2001, pp. 1–8.
[33] P. J. Curran, "Remote sensing of foliar chemistry," *Remote Sens. Environ.*, vol. 30, pp. 271–278, 1989.
[34] B. C. Gao, K. B. Heidebrecht, and A. F. H. Goetz, "Derivation of scaled surface reflectances from AVIRIS data," *Remote Sens. Environ.*, vol. 44, pp. 165–178, 1993.
[35] S. G. Ungar, J. S. Pearlman, J. Mendenhall, and D. Reuter, "Overview of the Earth Observing One (EO-1) mission," *IEEE Trans. Geosci. Remote Sensing*, vol. 41, pp. 1149–1159, June 2003.
[36] S. T. Gower and J. M. Norman, "Rapid estimation of leaf area index in conifer and broad-leaf plantations," *Ecology*, vol. 72, pp. 1896–1900, 1991.

Peng Gong received the B.S. and M.S. degrees from Nanjing University, Nanjing, China, in 1984 and 1986, respectively, and the Ph.D. degree from the University of Waterloo, Waterloo, ON, Canada, in 1990.

He is currently a Professor in the Department of Environmental Science, Policy and Management and Co-Director of the Center for Assessment and Monitoring of Forest and Environmental Resources, University of California, Berkeley. He was with York University, North York, and the University of Calgary, Calgary, AB, Canada, before joining the University of California, Berkeley in 1994. His research interests include photoecometrics, global change monitoring, and the role of technology on society. He is an author/coauthor of over 200 papers and five books. He serves as the Director of the International Institute for Earth System Science, Nanjing University.

Dr. Gong is Editor-in-Chief of *Geographic Information Sciences* and Editor of the *International Journal of Remote Sensing.*

Ruiliang Pu received the B.S. and M.S. degrees from Nanjing Forestry University (NFU), Nanjing, China, in 1982 and 1985, respectively, and the Ph.D. degree from the Chinese Academy of Sciences, Beijing, China, at the Department of Department of Environmental Science, Policy and Management (ESPM), University of California, Berkeley, in 2000.

Since 1995, he has been a Research Associate and currently is an Assistant Researcher at ESPM. He has been with NFU (1985–1990 and 1993) and was a Visiting Sientist at ISTS, York University, North York (1990–1991) and the University of Calgary, Calgary, AB, Canada, in 1994. His research interests include application of remote sensing in natural resources with an emphasis on the use of hyperspectral remote sensing data, multitemporal and multisensor data in evaluating productivity of forest land, and extracting forest canopy structure parameters (including both biophysical and biochemical parameters). He is an author/coauthor of over 60 papers.

Greg S. Biging received the B.S. and Ph.D. degrees from the University of Wisconsin, Madison in 1973 and 1978, respectively.

He is currently a Professor in the Department of Environmental Science, Policy and Management, University of California, Berkeley, and was the founding Director of the University of California, Berkeley's Center for Assessment and Monitoring of Forest and Environmental Resources. His research interests include forest biometrics and photoecometrics as well as map accuracy assessment. He is an author/coauthor of more than 80 papers including a book chapter and monograph on change detection accuracy assessment.

Mirta Rosa Larrieu received the B.S. degree from the Faculty of Agronomy, Buenos Aires University, Buenos Aires, Argentina, in 1980.

She has worked in Buenos Aires University for 16 years in the Forestry Department. She is currently the Coordinator of the Geographical Information System of the Forest Division of the Secretariat of Agriculture, Livestock, Fisheries and Food (SAGPyA) of Argentina, Buenos Aires, Argentina. She was in charge of the control of the execution of the First National Forest Plantation Inventory in the two-phase inventory basic cartography and field survey, and she is currently responsible in the permanent monitoring of all the forest plantations plans presented by forest producers to accede to the benefit of Forest Plantation Promotion System